Sindh Univ. Res. Jour. (Sci. Ser.) Vol. 45 (2) 453-460 (2013)

SINDH UNIVERSITY RESEARCH JOURNAL (SCIENCE SERIES)

Complex (RLC) Design Analysis Method of Zero Current Switching–Series Resonant Inverter High Voltage DC to DC Converter

A. AMIR, W. KUMAR[++], B. S. CHOWDHRY, A. AMIR*

Department of Electronic Engineering, Mehran University of Engineering & Technology, Jamshoro, Pakistan

Received 26th March 2013 and Revised 2nd June 2013

Abstract: The conventional Zero Current Switching– Series Resonant (ZCS-SR) circuit has almost zero switching losses. However, it has limitations in describing precise voltage gain values at instantaneous events as the parasitic components of the circuit remain neglected. This paper presents an improved analysis design method for the LC conventional ZCS-SR inverter high voltage dc power supplies, by considering the ideal parasitic components within circuit. Furthermore, the analysis of the circuit is carried out using complex RLC design. Considering these non-idealities, we have developed a complex valued analysis design model of ZCS-SR inverter high voltage dc-dc converter. This detailed model considers damping factors, parasitic losses and provides results for the entire cycle of operation. Simple analytical equations are derived, keeping the design techniques at large, to attain the essential performance parameters. This proposed analysis model has been simulated using PSPICE software. Results reveal that this analysis design model provides more than 80% efficiency.

Keywords: Complex analysis, complete cycle of operation, damping factor, inverter, parasitic losses, ZCS-SR converter.

1. INTRODUCTION

Efficiency, power density and switching frequency are the most important factors in modern power supplies. To achieve high efficiency, high switching frequency capabilities while keeping system design simple; resonant power supplies have been widely used nowadays (Lin *et al.,* 2011). Conventional ZCS-SR Converter is shown in Fig. 1 (Lin *et al.,* 2011, Honnyong *et al.,* 2010).These converters are widely used as power supplies in uninterruptible power systems (UPS), electronic appliances, biomedical equipment, automobile hybrid technology, Radio Frequency generation and Industries. Furthermore, these current-fed converters are found to be the best choice for the applications where high output voltages are required in response to low input voltages (Ajitha and Kalaiarasi, 2010, Iqbal *et al.,* 2008)

The conventional ZCS-SR converter, shown in **(Fig. 1),** is divided into six fractions: Inverter, Series Resonant circuit, Isolation Transformer, Diode Rectifier, Capacitive Filter and Load Resistance (Honnyong *et al.,* 2010). In this deign model; the inverter converts a Dc input into an Ac output. The Ac signal from the inverter is fed to Series resonant circuit. This fraction of the circuit is of prime importance as it provides resonance to the signal with an LC circuitry. Third fraction, isolation transformer, is used for both stepping up the voltage and for isolation between the Dc-Dc conversion circuits. The rectification of the output signal from secondary of the isolation transformer is performed by a bridge rectifier. Capacitor filters ripples in the signal provided by the rectifier. The resultant signal from the fifth fraction is fed to the load.

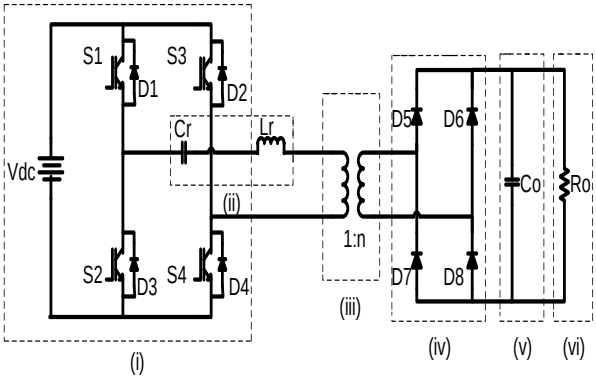

(i) Inverter, (ii) Series Resonant circuit, (iii) Isolation Transformer, (iv) Diode Rectifier, (v) Capacitive Filter, (vi) Load Resistance

Fig.1: Schematic diagram of the Zero Current S-SR inverter high voltage DC to DC converter

The parasitic losses, caused by leakage inductance, large turn`s ratio of the transformer with extensive insulation and winding capacitance, change the converter behavior and add non-idealities to the performance parameters (Johnson *et al.,* 1988, Iannello *et al.,* 2002, Weinberg and Schreuders, 1986, Krichtafovitch and Sinitsyna, 1994). Slow rise time and current spikes are caused by the winding capacitance. Moreover, the leakage inductance provides heavy voltage spikes. The consideration of these parasitic

[++]Corresponding Author: Wanod Kumar, email: wanod.kumar@faculty.muet.edu.pk
*Institute of Information and Communication Technology, University of Sind, Pakistan

components in the analysis design model can result into aggrandized efficiency and high reliability (Lin *et al.,* 2011).

Following the introduction the rest of the paper is organized as follows: Section 2 details the related work. Proposed design analysis model is given in Section 3. Section 4 describes the operational modes of the circuit. The performance evaluation of the system is carried out in Section 5. Paper concludes in Section 6.

2. RELATED WORK

The exclusion of the parasitic components in ZCS-SR analysis design (i.e. the parasitic capacitance not integrated or the leakage inductance ignored) causes non idealities in desired results (Lin *et al.,* 2012, Kim *et al.,* 1995, Iannello *et al.,* 2002). Furthermore, these parasitic losses were untouched in system design analysis in previous research while (Lin *et al.,* 2012, Martin-Ramos *et al.,* 2005, Martin-Ramos *et al.,* 2007, Lin *et al.,* 2011) being the exception. In (Sze Sing *et al.,* 2012, Sze Sing *et al.,* 2011), the authors have proposed a multi output ZCS-SR inverter to structure the LC changes for wide variety of outputs. However, they have ignored the parasitic losses, instantaneous analysis and damping which in turn affects system analysis design efficiency. An Ac analysis of the converter based on the fundamental frequency model is presented in (Prabhakar *et al.,* 2009), yet lacks with the inclusion of parasitic losses and so, ignores the damping effect. Dc analysis modeling of the ZCS-SR with parasitic components is presented in (Martin-Ramos *et al.,* 2005, Martin-Ramos *et al.,* 2007). However, complex modeling (due to the imaginary and real values of the components) is ignored and so, an ac analysis remains untouched. In (Lin *et al.,* 2012, Lin *et al.,* 2011), LC analyses of systems using first harmonic analysis (FHA) with parasitic components while ignoring the instantaneous analyses are presented. Hence, the consideration of entire cycle of operation would have resulted in better system analysis.

To overcome the above mentioned limitations, we in this paper, propose a detailed analysis system design by considering.

- Instantaneous values of each parameter
- Damping factor inclusion
- Complex analysis of a resonant converter along with the consideration of the parasitic components. The required resonant elements are proposed with R (resistance) as the ideal parasitic element
- Entire cycle of operation.

3. PROPOSEDDESIGN ANALYSIS MODEL

Pspice simulation results in terms of resonant voltage and current of the converter are shown in **(Fig.2).** Waveforms clearly depict the alternating nature. Therefore, it is necessary to consider damping factor, phase angle, real and imaginary (complex) values of components including the parasitic components, peak voltages and peak currents to have complete instantaneous analysis.

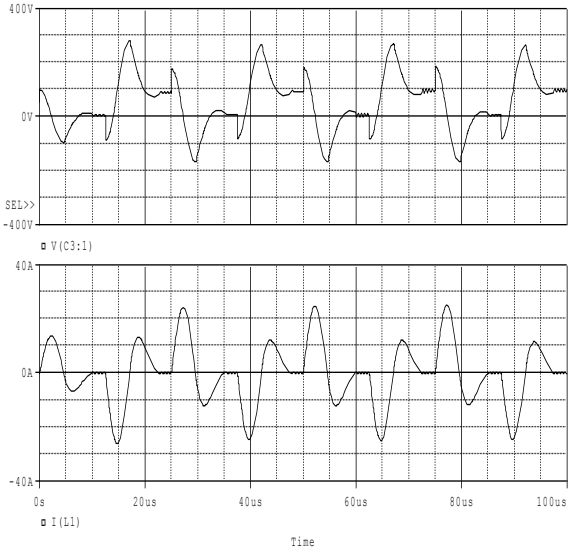

Fig.2: Plots of Resonant capacitor and inductor for the ZCS-SR converter.

To achieve better accuracy and high efficiency of the system design, in this section we analyze the tank circuit including the idealistic parasitic components through the RLC complex model (Lin *et al.,* 2012). The equivalent circuit of LC resonant converter including parasitic components (RLC)is depicted in Fig.3 (Lin *et al.,* 2011). In this design model, Cr is the capacitance and Lr is the inductance for the imaginary analysis. The inclusion of resistance (R) of the circuit results in a complex analysis presenting the parasitic components.

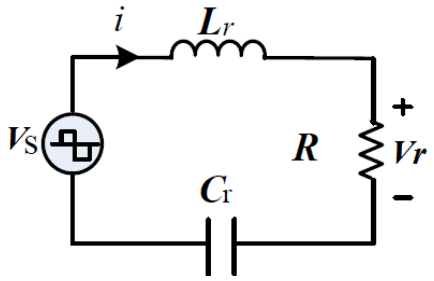

Fig.3: Equivalent circuit of LC resonant converter including parasitic components.

The angular resonant (ω_r) and switching frequencies are given by:

$$\omega_r = \frac{2\pi}{T_r} = 2\pi f_r$$

$$f_s < 0.5 f_r$$

The supply voltage (V_S)is

$$V_S = Ri(t) + \frac{1}{Cr}\int_{t_o}^{t} i\,(t)\,dt + L_r\frac{di\,(t)}{dt} + V_p \quad (1)$$

The roots of this RLC circuit are

$$S = R \pm \omega_r i \quad (2)$$

where $\omega_r = \frac{1}{\sqrt{LC}}$ and $i = \sqrt{-1}$.

Fig. 4 represents the step response of the circuit, obtained through MATlab. Due to the parasitic components, the damping effect can be observed in the step response.

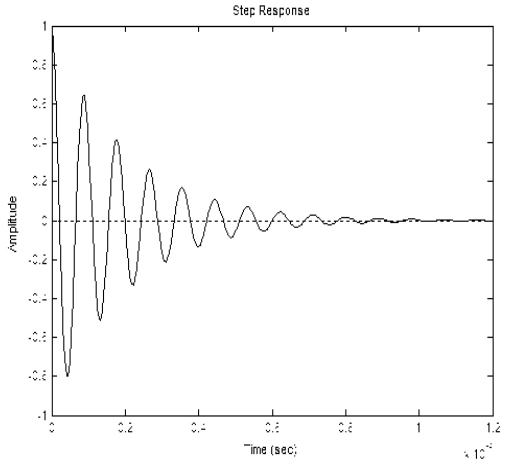

Fig. 4: Step response for the proposed model in MATlab.

The total resonant current is

$$I(t) = \frac{V_{max}\,\cos(\omega_r t - \emptyset)}{|Z|} + Icomp \quad (3)$$

where V_{max} is the peak voltage and$Icomp$ is the imaginary part of the resonant current, which is defined as

$$Icomp = (A_1\, e^{-\alpha t}\cos\omega_r t) + (A_2\, e^{-\alpha t}\sin\omega_r t) \quad (4)$$

where α represents the damping factor as observed in Fig.4. The circuit impedance (Z) is shown in **(Fig. 5)** using vector diagram.

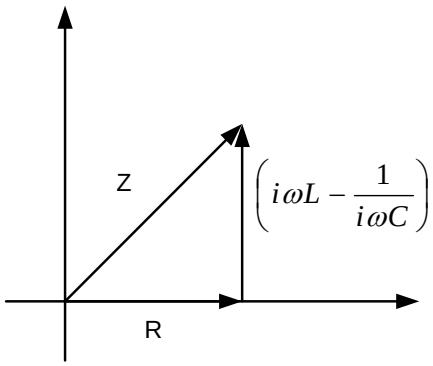

Fig.5: Vector diagram of resonant electrical parameters.

The amplitude and the phase of Z are

$$|Z| = \sqrt{(R^2 + (\omega L - \tfrac{1}{\omega C})^2} = 2\omega_r L$$

$$\emptyset = tan^{-1}\frac{\omega L - \frac{1}{\omega C}}{R}$$

At t=0, the $Icomp$ becomes

$$Icomp = 0 + A_2$$

where $A_2 = \frac{V_{in} + \frac{V_o}{n}}{\omega_r L}$ *and* $A_1 = 0$.

Now, the total resonant current becomes

$$I(t) = \frac{V_{max}\,\cos(\omega_r t - \emptyset)}{|Z|} + \frac{V_{in} + \frac{V_o}{n}}{\omega_r L}$$

$$I(t) = \frac{V_{max}\,\cos[\omega_r(t) - \varphi]}{2\omega_r L} + \frac{V_{max}\,(\cos\omega_r t) + \frac{V_{\circ max}\,(\sin\omega_r t)}{n}}{\omega_r L} \quad (5)$$

and total capacitor voltage is

$$V_C(t) = \frac{-1}{C}\left[\begin{matrix} V_{max}\left(\frac{\sin\omega_r(t)\cos\emptyset}{2\omega_r L} - \frac{\cos\omega_r(t)\sin\emptyset}{2\omega_r L}\right) \\ + \\ V_{max}\,\frac{\sin\omega_r(t)}{{\omega_r}^2 L} + \frac{V_{\circ max}\cos\omega_r(t)}{n{\omega_r}^2 L} \end{matrix}\right] + \mathrm{K} \quad (6)$$

where K=$-V_C'$is the integration constant. V_C' is the initial capacitor voltage and is given by:

$$V_C' = \frac{V_{\circ max}}{n} \quad (7)$$

where $V_{\circ max}$ represents peak output voltage.V_{Cmax} , the initial peak charged capacitor voltage, is defined as:

$$V_{Cmax} = \frac{V_{max}\ sin\varphi}{2} \quad (8)$$

This complex analysis is not limited to the first harmonic or the first cycle (Lin *et al.*, 2012), but extends to the entire cycle of operation. For its complete analysis modes of operation have been established as shown in Fig. 6 (An enlarged representation of Fig. 2.

In all, most of the analysis till yet on ZCS-SR converters had been on considering the LC resonant circuit making it an imaginary analysis, whereas ignoring the parasitic components. For this purpose a complete system design while considering the parasitic components is presented here with complex analysis.

4. OPERATIONAL MODES

Analysis of this converter is carried out using phase shifted PWM method where the switches (S1, S2, S3, and S4) are employed in a diagonal fashion. **(Fig.6)** shows the steady-state values of resonant inductance current and capacitor voltage with the ideal considerations of parasitic components. Moreover a detailed analysis is provided for both charged and discharged capacitor cases for all operational modes.

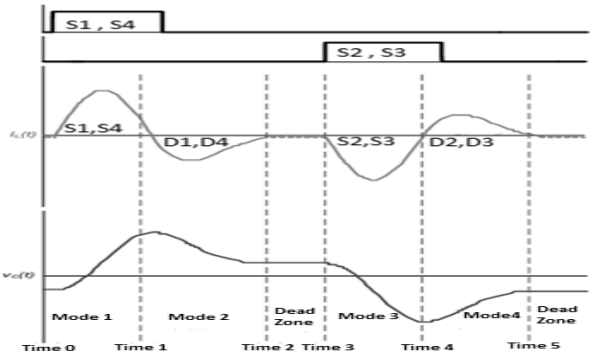

Fig. 6: Steady-state waveform of the proposed system for resonant inductance and capacitance current and voltage.

a) Mode I

During the positive half cycle (t_0-t_1), the switches S_1 and $S_4$are functioning and allow current to flow from the input to tank circuit. At t_0, S_1 and S_4 are switched ON by zero current (supplied by reverse diodes). Further, S_1 and S_4turn OFF at $t_1$as current becomes zero. Resulting output is supplied to load by the D_C source. The complete operation of Mode I is shown in **Fig. 7(a).** When S1 and S4 are ON remaining switches are OFF.

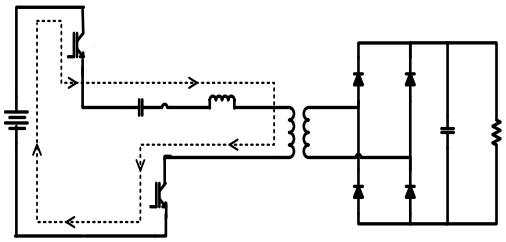

Fig.7(a): The equivalent circuit of Mode I

DISCHARGED Capacitor:

$$i_L(t) = \left(\frac{V_{in} + \frac{V_o}{n}}{\omega_r L}\right) e^{-\alpha t} \sin \omega_r t\,, t_\circ < t < t_1 \quad (9)$$

$$V_c(t) = (V_{in} + \frac{V_o}{n})[1 - e^{-\alpha t}\{(\alpha/\omega r)\sin + cos\omega rt\}] - \frac{V_{\circ max}}{n}, \quad t_\circ < t < t_1 \quad (10)$$

CHARGED Capacitor:

$$i_L(t) = \left(\frac{V_{in} + V_c' + \frac{V_o}{n}}{\omega_r L}\right) e^{-\alpha t} \sin \omega_r t\,, t_\circ < t < t_1 \quad (11)$$

$$V_c(t) = (V_{in} + \frac{V_o}{n}) + ([(V_{in} + \frac{V_o}{n} + \frac{V_{\circ max}}{n})[1 - e^{-\alpha t}\{(\alpha/\omega r)\sin\omega_r t + cos\omega rt)\}] - \frac{V_{\circ max}}{n}, t_\circ < t < t_1 \quad (12)$$

b) Mode II

The operation of Mode II is shown in **Fig.7(b).** From (t_1-t_2), the current flows back through the reverse diodes. Bidirectional energy flow cannot occur as diodes D_1 and D_4 (connected in anti-parallel) only permit unidirectional energy transfer. The switches S_1 and S_4remain OFF under ZCS condition. In this mode, D_1 and $D_4$are ON while rest are OFF.

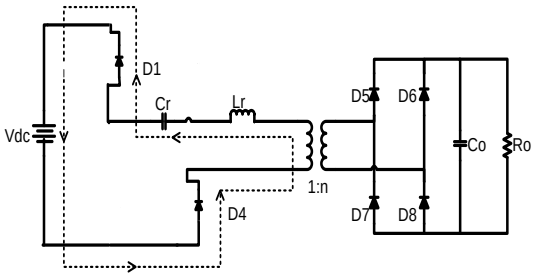

Fig. 7 (b): The equivalent circuit of Mode II

DISCHARGED Capacitor:

$$i_L(t) = \left(\frac{V_{in} - V_{cmax} + \frac{V_o}{n}}{\omega_r L}\right) e^{-\alpha t} \sin \omega_r t, t_1 < t < t_2 \quad (13)$$

where

$$0, t_2 < t < t_3 (Dead\ Zone)$$

$$V_c(t) = (V_{in} + \frac{V_o}{n}) - \left(\left[(V_{in} + \frac{V_o}{n}\right] - \frac{V_{max}\ sin\varphi}{2}\right)[1 - e^{-\alpha t}\{(\alpha/\omega r)\sin\omega_r t + cos\omega rt)\}] \frac{V_{max}\ sin\varphi}{2} \quad t_1 < t < t_2 \quad (14)$$

where

$$V_c^{'}, t_2 < t < t_3 (Dead\ Zone)$$

CHARGED Capacitor:

$$i_L(t) = \left(\frac{V_{in} - \frac{V_o}{n}}{\omega_r L}\right) e^{-\alpha t} \sin \omega_r (t - t_1), t_1 < t < t_2 \quad (15)$$

$$V_c(t) = (V_{in} - \frac{V_o}{n})[1 - e^{-\alpha t}\{(\alpha/\omega r)\sin\omega_r (t - t_1) + cos\omega r(t - t_1)\}] + \frac{V_{max}\ sin\varphi}{2}, \quad t_1 < t < t_2 \quad (16)$$

c) Mode III

During the negative half cycle, S_2 and S_3turn ON and the D_C output is supplied to the load resistance from time (t_3-t_4). **Fig.7(c)** represents the operation of Mode III, where only S_2 and S_3 remain ON.

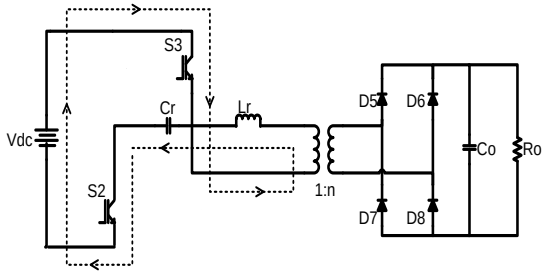

Fig. 7(c): The schematic of Mode III

CHARGED Capacitor:

The simulation results show that mode III only operates with charged capacitor condition.

$$i_L(t) = -\left(\frac{V_{in} + V_c' + \frac{V_o}{n}}{\omega_r L}\right) e^{-\alpha t} \sin \omega_r (t - \frac{T_s}{2}),\ t_3 < t < t_4 \quad (17)$$

$$V_c(t) = -(V_{in} + \frac{V_o}{n}) - \left(\left[(V_{in} + \frac{V_o}{n}\right] + \frac{V_{cmax}}{n}\right)[1 - e^{-\alpha t}\{(\alpha/\omega r)\sin\omega_r t + cos\omega rt)\}] + \frac{V_{cmax}}{n}\ t_3 < t < t_4 \quad (18)$$

d) Mode IV

From (t_4-t_5) the stored energy during mode-III flows in the reverse direction. The diodes D_2 and D_3 (connected in anti-parallel) with the switches $S_2$and S_3block the reverse flow of current, hence, turning OFF switches $S_2$and S_3underzero current condition. As shown in Fig.7(d), D2 and D3 are ON remaining are OFF, The simulation results show that mode IV only operates with discharged capacitor condition.

Please note that Mode II and Mode IV have current through the diodes in opposite direction, the equations for charged and discharged are mirror images of each other or reciprocals.

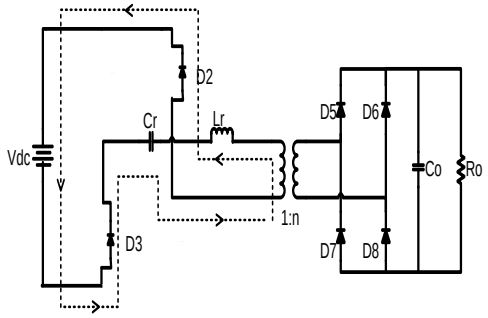

Fig. 7(d): The equivalent circuit of Mode IV

DISCHARGED Capacitor:

$$i_L(t) = -\left(\frac{V_{in} - \frac{V_o}{n}}{\omega_r L}\right) e^{-\alpha t} \sin \omega_r (t - t_1), t_4 < t < t_5 \quad (19)$$

where

$$0, t_5 < t < t_6\ (Dead\ Zone)$$

$$V_c(t) = -(V_{in} + \frac{V_o}{n}) + \left(\left[(V_{in} + \frac{V_o}{n}\right] - \frac{V_{max}\ sin\varphi}{2}\right)[1 - e^{-\alpha t}\{(\alpha/\omega r)\sin\omega_r t + cos\omega rt)\}] - \frac{V_{max}\ sin\varphi}{2} t_4 < t < t_5 \quad (20)$$

where

$$-V_c^{'}, t_5 < t < t_6 (Dead\ Zone)$$

5. PERFORMANCE EVALUATION

The conventional ZCS-SR converter with imaginary resonant values without considering the values of parasitic components is shown in **Fig.8 (a)** with a pole zero representation. This can be observed that the poles are on imaginary axis; hence this analysis ignores the resistive effect of parasitic elements. **Fig.8 (b)** shows the pole zero map for the analysis of the converter including parasitic components. It clearly shows that the inclusion of the parasitic components in the circuit causes damping effect.

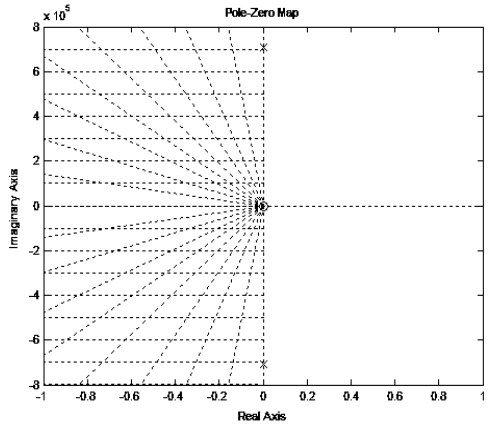

Fig. 8(a). Pole zero representation of the conventional converter.

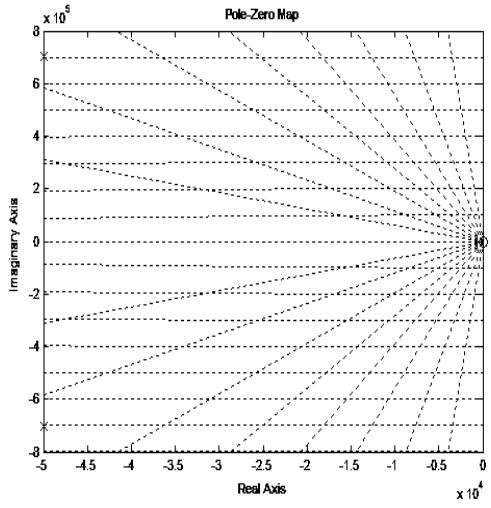

Fig.8(b). Pole zero representation of the proposed converter.

The simulation results of the converter including losses are shown in Figures 9 and 10. For a better understanding of the system design, we have considered two sets of parameters in this paper.

In first case **(Fig. 9)** the performance results (in terms of Resonant capacitive voltage and inductance current) are obtained using following parameters: Input voltage (V_{DC})= 100 V dc, Resonant capacitance(Cr) = 200nF, resonant inductance (Lr) = 10uF,Switching Frequency (f_S) = 40 kHz, Resonant Frequency (fr) = 112kHz, Load resistance (R_o)= 150kΩ. These parameters have been carefully taken to attain the desired dc output. The values of output voltage and the peak current are 4.1kV and 22.5A at resonance respectively. Furthermore, we have determined the values of resonant capacitive voltage and inductance current using mathematical analysis. The simulation results are in good agreement with analytical results. Compared to previous analysis proposed in literature, our analysis design method achieves more than 80% efficiency considering both analytical and simulation results.

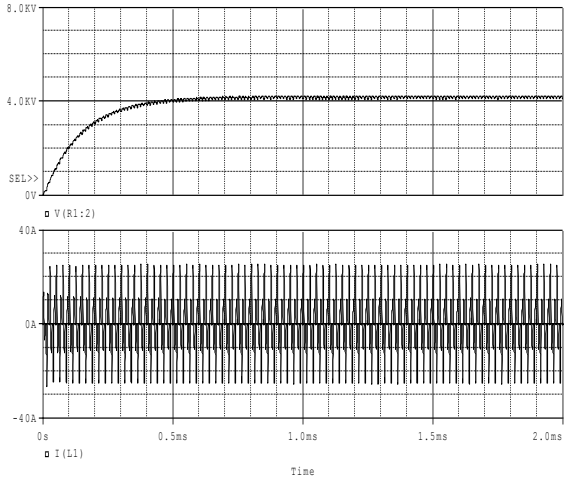

Fig. 9: Simulation result of output voltages &currents of proposed converter for R_o= 150kΩ.

Mode I Discharged

$$\{ i_L(0) = 0, i_L\left(\frac{\pi}{2}\right) = 15.1\ A, i_L(\pi) = 0\}$$
$$\{V_c(0) = 0, V_c\left(\frac{\pi}{2}\right) = -99.1\ V, V_c(\pi) = 0\}$$

Mode II Discharged

$$\{ i_L(\pi) = 0, i_L\left(\frac{3\pi}{2}\right) = -6.94A, i_L(2\pi) = 0\}$$
$$\{V_c(\pi) = 0, V_c\left(\frac{3\pi}{2}\right) = -101.1\ V, V_c(2\pi) = 0\}$$

Mode I Charged

$$\{ i_L(0) = 0, i_L\left(\frac{\pi}{2}\right) = 20.3\ A, i_L(\pi) = 0\}$$
$$\{V_c(0) = 0, V_c\left(\frac{\pi}{2}\right) = 230.7\ V, V_c(\pi) = 0\}$$

Mode II Charged

$$\{ i_L(\pi) = 0, i_L\left(\frac{3\pi}{2}\right) = -12.3A, i_L(2\pi) = 0\}$$
$$\{V_c(\pi) = 0, V_c\left(\frac{3\pi}{2}\right) = 161.1\ V, V_c(2\pi) = 0\}$$

Mode III Charged

$$\{ i_L(0) = 0, i_L\left(\frac{\pi}{2}\right) = -20.3\ A, i_L(\pi) = 0\}$$
$$\{V_c(0) = 0, V_c\left(\frac{\pi}{2}\right) = -230.7\ V, V_c(\pi) = 0\}$$

Mode IV Charged

$$\{ i_L(\pi) = 0, i_L\left(\frac{3\pi}{2}\right) = 12.3\ \text{A}, i_L(2\pi) = 0\}$$
$$\{V_c(\pi) = 0, V_c\left(\frac{3\pi}{2}\right) = -100.1\ V, V_c(2\pi) = 0\}$$

In second case we consider a load resistance (R_O) of 500kΩ. The Fig.10 shows that the output voltage is 11kV and peak current is 25A at resonance. Moreover, these results can be verified through

equations of each mode for the complete cycle of operation.

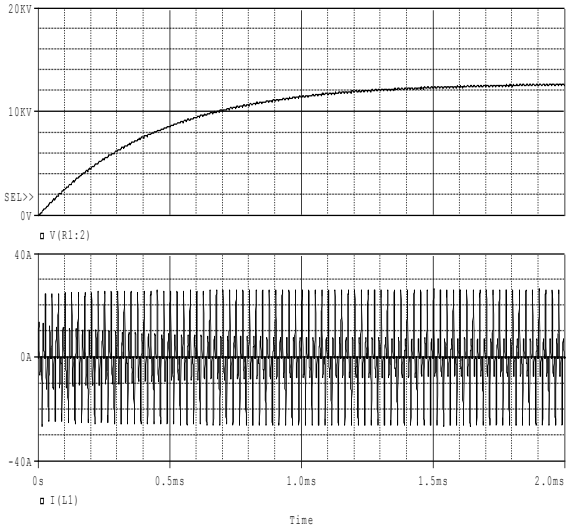

Fig.10: Simulation result of output voltages& currents of proposed converter for R_o= 500kΩ.

These results verify the accuracy of the proposed complex analysis of the converter for a complete cycle of operation (with instantaneous values) along with the damping factor compensations.

6. CONCLUSION

Previous analysis work on LC resonant converters does not completely explain practical behavior of design as parasitic losses remain untouched. Further, the consideration of parasitic components in the analysis for an entire cycle of operation makes the system design more practical. To confront these issues, a complex method is proposed considering the following:

- Instantaneous analysis including the damping factor
- Phase angle, impedance, real and imaginary (complex) values of components.
-
- The parasitic elements
- Peak voltages and peak currents
- AC analysis for the resonant circuit

The results prove the accuracy of our proposed analysis. An efficiency of more than 80% for the entire cycle of operation has been achieved while considering the ideal parameters of the parasitic elements within the tank network.

ACKNOWLEDGEMENTS

The authors acknowledge the Mehran university of Engineering and Technology, Jamshoro, Pakistan, for providing laboratory and research facilities.

REFERENCES:

Ajitha, S. and N. Kalaiarasi, (2010) Article: Implementation Of Full-Bridge Current-Fed Resonant Boost Converter Using Pic Microcontroller. *International Journal Of Computer Applications,* 1**,** 76-81.

Honnyong, C., F. Z. Peng, and Y. Dongwook, (2010) Source Resonant Dc-Dc Converter For Wide Input Voltage And Load Variation. *In:* Power Electronics Conference (Ipec), 2010 International, 21-24 June 2010. 995-1000.

Iannello, C., L. Shiguo, and I. Batarseh, (2002) Full Bridge Zcs Pwm Converter For High-Voltage High-Power Applications. *Aerospace And Electronic Systems, Ieee Transactions On,* 38**,** 515-526.

Iqbal, S., G. K. Singh, & R. Besar, (2008) A Dual-Mode Input Voltage Modulation Control Scheme For Voltage Multiplier Based X-Ray Power Supply. *Power Electronics, Ieee Transactions On,* 23**,** 1003-1008.

Johnson, S. D., A. F. Witulski, and R. W. Erickson, (1988) Comparison Of Resonant Topologies In High-Voltage Dc Applications. *Aerospace And Electronic Systems, Ieee Transactions On,* 24**,** 263-274.

Kim, Y. J., M. Nakaoka, H. Takano, and T. Hatakeyama, (1995) Comparative Performance Evaluations Of High-Voltage Transformer Parasitic Parameter Resonant Inverter-Linked High-Power Dc-Dc Converter With Phase-Shifted Pwm Scheme. *In:* Power Electronics Specialists Conference, 1995. Pesc '95 Record., 26th Annual Ieee, 18-22 Jun 1995. 120-127.

Krichtafovitch, I. A. and I. Z. Sinitsyna, (1994) Theory and Design of High-Voltage Power Supplies. *In:* High Frequency Power Conversion (Hfpc) Conference, 1994. 147-157.

Lin, W., W. Jun, J. Meng, L. Wei, L. Zhigang, and Z. Shutian, (2011) An Improved Design Method For Lc Resonant Converter Considering Effects Of Parasitic Components. *In:* Electrical Machines And Systems (Icems), 2011 International Conference On, 20-23 Aug. 2011. 1-4.

Lin, W., W. Jun, L. Zhigang, and Z. Shutian, (2012) Analysis and Design Of Lc Series Converter Considering Effect Of Parasitic Components. *In:* Computer Distributed Control and Intelligent Environmental Monitoring (Cdciem), 2012 International Conference On, 5-6 March 2012. 126-130.

Martin-Ramos, J. A., J. Diaz, A. M. Pernia, J. M. Lopera, and F. Nuno, (2007) Dynamic And Steady-State Models For The Prc-Lcc Resonant Topology With A Capacitor As Output Filter. *Industrial Electronics, Ieee Transactions On,* 54**,** 2262-2275.

Martin-Ramos, J. A., A. M. Pernia, J. Diaz, F. Nuno, and J. M. Alonso, (2005) A Circuit For The Large And Small Signal Dynamic Modeling of The Prc-Lcc Resonant Topology With A Capacitor As Output Filter. *In:* Power Electronics Specialists Conference, 2005. Pesc '05. Ieee 36th, 16 June 2005. 635-641.

Prabhakar, M., S. Arulmozhi, and V. Kamaraj, (2009) Selection Criteria and Analysis of Lcc Resonant Dc–Dc Converters For Automotive Applications. *Modern Applied Science,* 3**,** 21-31.

Sze Sing, L., S. Iqbal, and M. Kamarol, (2011) A Digitally Tuned Resonant Capacitance Control With Narrow Range Frequency Modulation For Zcs High Voltage X-Ray Power Supply. *In:* Electrical, Control And Computer Engineering (Inecce), 2011 International Conference On, 21-22 June 2011. 113-118.

Sze Sing, L., S. Iqbal, and M.Kamarol, (2012) Control of Zcs-Sr Inverter-Fed Voltage Multiplier-Based High-Voltage Dc–Dc Converter By Digitally Tuning Tank Capacitance And Slightly Varying Pulse Frequency. *Power Electronics, Ieee Transactions On,* 27**,** 1076-1083.

Weinberg, A. H. and J. Schreuders, (1986) A High-Power High-Voltage Dc-Dc Converter For Space Applications. *Power Electronics, Ieee Transactions On,* Pe-1**,** 148-160.